Atkinson and Huang *Mathematics-in-Industry Case Studies* (2016) 7:3
DOI 10.1186/s40929-016-0003-6

Mathematics-in-Industry
Case Studies

RESEARCH Open Access

A theoretical model for capacitance measurement of liquid films in an annular flow

Colin Atkinson[1,2*] and Ruoxi Huang[3]

* Correspondence: atkinson2@slb.com
[1]Schlumberger Gould Research Center, Cambridge, UK
[2]Department of Mathematics, Imperial College London, 180 Queen's Gate, London SW7 2AZ, UK
Full list of author information is available at the end of the article

Abstract

This paper develops mathematical models for a proposed production logging tool, which uses capacitance sensors to measure liquid annulus thickness and liquid type for a primarily gas-carrying wellbore. A semi-analytical method is devised which uses Fourier analysis to account for the complicated system geometry and reduces the problem to singular integral equations over a sensor electrode. Approximate solutions of these integral equations give expressions for capacitance, which is calculated for different liquids and varying liquid annuli thicknesses and electrode positions. These results are compared with capacitance values found using COMSOL Multiphysics, a finite element package. Good agreement is obtained between these two methods, with a discrepancy range of 1–8 %. Capacitance values obtained range from 32 to 93 pF/m, and sensitivity is estimated to range from 0.8 to 60 %, depending mainly on the proximity of the electrode to the liquid and also on the permittivity and thickness of the liquid layer. Practical implications of the study are also discussed. Realistically useful measurements, where ~0.2 mm of liquid is detectable, can potentially be made using an electrode 4–6 mm away from the inner wellbore wall.

Introduction

In oil and gas production, a technical service known as production logging (PL) is used to identify different fluid phases in the wellbore and measure the flow rates of each. A sensor carrying tool can be deployed downhole to measure production rates at different depths, so that entry points of fluid flow can be located. This serves as a useful diagnostic tool and can help with well management.

A well producing primarily gas with a small amount of liquid, which could be oil, water or sometimes a mixture of both, is likely to have an annular flow regime, with the liquid phase forming a thin annulus on the inside wall of the pipe and the gas flowing in the form of a central core. While the gas flow rate can be measured with existing PL sensors [1], the thin liquid layer, which may contain more valuable oil, is more difficult to detect and measure using conventional equipment. A PL tool that can detect and identify this liquid could, for example, find water-producing zones to be blocked and find areas of oil-bearing formation to be further exploited.

Recently, a PL tool based on inside-out capacitance tomography has been described [2], which uses measurements of capacitance between multiple electrodes mounted

around the circumference of a cylinder-shaped tube, and between these electrodes and the steel casing wall of the borehole. However, since the sensing electrodes are on a small diameter tool body (42 mm) centralised in a large diameter wellbore (e.g. 150 mm), it is unclear whether such an arrangement is sensitive enough for the purpose of measuring a thin liquid layer on the casing wall.

We propose a different measurement arrangement, in which a deployment mechanism is used to place capacitive sensing electrodes closer to the casing, in order to improve the sensitivity of liquid detection. The key aims of the study are to create a model of a simplified version of this system (Fig. 1) to predict capacitance measurements and to gain insight into factors affecting these values. Other important questions that this study attempts to answer include the following:

- From a capacitance measurement, can we derive both the liquid layer thickness and the liquid type (i.e. oil or water)?
- How close to the casing must the electrodes be to detect capacitance changes due to the presence of a thin liquid layer (bearing in mind that capacitance changes much smaller than 0.1 pF are difficult to measure with electronics in down-hole conditions)?
- Given the electrode-casing separation, what are the minimum liquid layer thicknesses that the sensor can detect for oil and water?

In Fig. 1, the casing and tool are grounded and the electrodes are held at an electric potential of $\pm V_0$. Capacitance values between the electrodes and casing are converted into a voltage signal through a capacitance-to-voltage converter circuit. The dimensions used are industry standards, with a 6–7 in borehole casing diameter and a logging tool

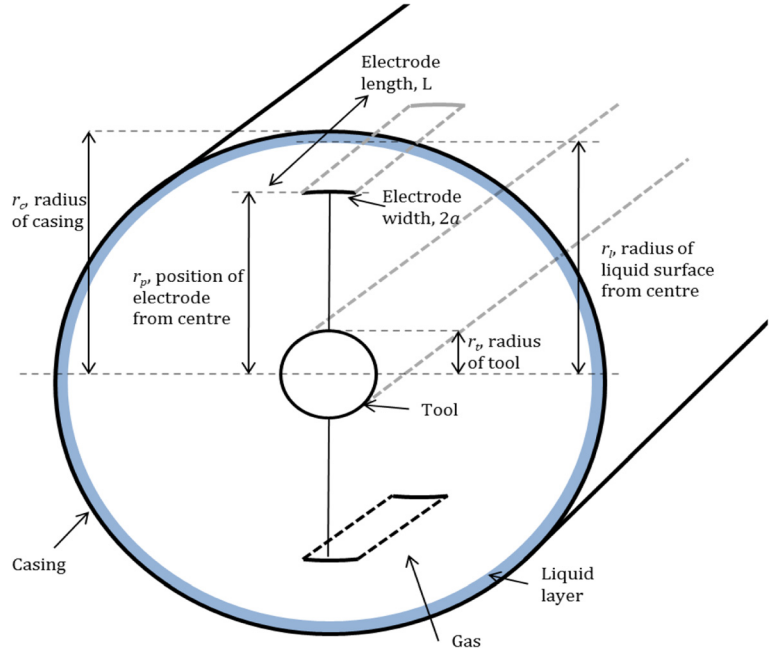

Fig. 1 Diagram of the geometry of the measurement system

of $1\frac{11}{16}$ inch diameter. The electrode is modelled to have a width of 15 mm and a length along the casing, L. The range of the liquid layer thickness is between 0 and a few millimetres, defined by a typical annular flow of interest. Three liquids of different permittivities were used in the study: water (high permittivity), oil (low permittivity) and salt water (conductive).

The system was viewed in two different 2D geometries which were used to develop capacitance models both theoretically and by using a finite element computation package, COMSOL Multiphysics® [3]. The first geometry used was a simplification of the system into a planar form, where the electrodes and boundaries lie flat and parallel (see the section 'Adaptation from real geometry', Fig. 2). The theory gives a relatively simple solution and so can provide a faster computation of capacitance. A cross section of the system was used as the second model geometry (see the section 'Geometry', Fig. 7), which has concentric boundaries with curved electrodes.

For each of these geometries, mathematical models were derived using general solutions for electrostatic potential satisfying Laplace's equation and the boundary conditions within the system. The electrode's potential was equated with the integral of a continuous distribution of point source potentials on the electrode. From this singular integral equation, we solve for the charge density distribution and thus the capacitance. These models calculate capacitances for different liquids, varying electrode positions, and liquid layer thicknesses for a given set of system parameter values. The analytical expressions obtained provide insight into the dependence of capacitance on the parameters of the system and the liquid layer, and also, the high speed of calculation is optimal for real-time analysis as the PL tool is lowered down the well.

To test the accuracy of the developed theory, the models of the system were then built with a fine mesh in COMSOL, using the Electrostatics module, and capacitance values were calculated for varying liquid thicknesses by using parametric sweep studies.

The background theory behind the mathematical models is detailed in the next section; sections 'Planar model' and 'Circular model' cover the theoretical (sections 'Theoretical model' and 'Theoretical model') and COMSOL (sections 'COMSOL multiphysics model' and 'COMSOL model') models for the planar system and the circular cross section system, respectively, and include results and comparisons of the calculations of capacitance (sections 'Results and comparison' and 'Results and comparison'). The section 'Overall conclusions' summarises the main conclusions of this paper, the 'Acknowledgements'

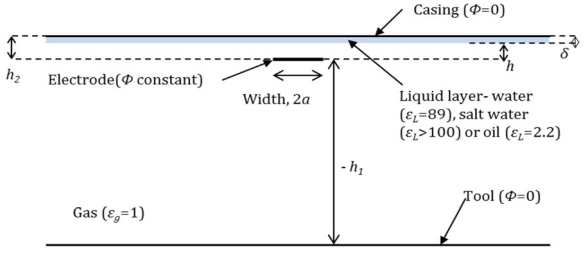

Fig. 2 Diagram of the planar model showing the boundary conditions for the potential, Φ. h_1 is the distance of the electrode from the tool, h_2 is the distance of the electrode from the casing wall, h is the distance of the liquid layer from the electrode and the width of the electrode is 2a

section acknowledges those who have contributed to the study, and the 'References' section includes a list of references.

Background theory

The theoretical methods devised are based on solving for the distribution of potential sources along the electrode plate, the integral of which is related to the charge on the plate. The potential of a point source in two dimensions is given by $\phi^* = \ln r$ where r is the distance from the source. The presence of boundaries creates image sources which contribute an interaction potential term. This term may be quite complicated due to the different natures and geometries of the boundaries and the geometry of the source and therefore the potential cannot be solved in closed form. This interaction potential term is called U throughout the paper and the total potential due to a point source and the boundaries is referred to as ϕ. The total potential due to the distribution of sources and interaction potentials is Φ.

As the potential on the electrode is a predefined constant, V_0, a singular integral equation (see, for example, [4]) can be formed when setting the potential at the plate to V_0. This will have the form of Eq. (1),

$$\Phi_{\text{electrode}} = \int_{\text{electrode}} f(\xi)\ \ln|x-\xi|\ d\xi\ +\ \int_{\text{electrode}} f(\xi)\ U\ d\xi = \ V_0 \tag{1}$$

where ξ is the position of a point source on the electrode and x is position along the electrode.

It can be shown that for a single electrode plate in an infinite medium, i.e. when $U = 0$, this integral equation can be solved exactly with the flux density $f(\xi)$ having a square root singular form as ξ approaches the ends of the plate. The integral equation will be more complicated when other boundaries are present, and so these need to be solved using approximation methods. In general, for a plate at $-a < x < a$,

$$f(\xi) = \frac{F(\xi)}{\left(a^2-\xi^2\right)^{\frac{1}{2}}} \tag{2}$$

The crudest approximation method, which is used to develop the models in this paper, assumes that $F(\xi)$ is a constant, F. A more accurate method could be developed by approximating the unknown function $F(\xi)$ either pointwise or by an expansion in Chebyshev polynomials (for example, see [5]). The integral of this charge density distribution over the electrode is defined to be Q

$$Q = \int_{\text{electrode}} f(\xi)\, d\xi \tag{3}$$

And so, assuming $F(\xi)$ is constant, F, Eq. (3) becomes

$$Q = \pi F \tag{4}$$

The first theoretical method approximates the effect of the boundaries on the plate as though the image sources were induced by a point source of strength Q, see (3), at the centre of the plate, so that U does not depend on ξ. This method is accurate provided that the plate is far enough from the

boundaries and will be referred to as the point strength method. The second more accurate method requires solving the complete integral equation by integrating both sides over the electrode. The theoretical results are computed using these models.

The charge on the plate can be found from Maxwell's first equation in 2D (Eq. (5)), where E is the electric field, $\hat{\underline{n}}$ is the unit vector normal to the closed boundary, l, of S, q is the charge enclosed in the surface S, ε_r is the relative permittivity and ε_0 is the permittivity of free space.

$$\int_S \underline{\nabla}\cdot\underline{E}\ dS = \frac{q}{\varepsilon_0\varepsilon_r} \tag{5}$$

Using Gauss' law in 2D, this can be expressed by

$$\oint_l \underline{E}\cdot\hat{\underline{n}}\ dl = \frac{q}{\varepsilon_0\varepsilon_r} \tag{6}$$

When the surface encloses no free charge, the electrostatic potential Φ must satisfy Laplace's equation, below, since $\underline{E} = -\underline{\nabla}\Phi$.

$$\nabla^2\Phi = 0 \tag{7}$$

Assuming l encloses a charged flat plate extending along $-a < x < a$ on $y = 0$, Eq. (6) becomes

$$\int_{-a}^{a} \left(E_{y|y=0^+} - E_{y|y=0^-}\right)\ dx = \frac{q}{\varepsilon_0\varepsilon_r} \tag{8}$$

where $E_{y|y=0^\pm}$ is the y component of the electric field on the top or bottom of the plate. Using $\underline{E} = -\underline{\nabla}\Phi$, we can express this as

$$-\int_{-a}^{a} \left[\frac{\partial\Phi}{\partial y}\right]_{y=0^-}^{y=0^+} dx = \frac{q}{\varepsilon_0\varepsilon_r} \tag{9}$$

The charge on the plate is related to the jump in the derivative of the potential across the plate. The interaction term U will be continuous across the plate, and so the discontinuity is due to the derivative of the ln$r$ term. Differentiating the first term of Eq. (1) gives

$$\frac{\partial\left(\int_{\text{electrode}} f(\xi)\ \ln r\ d\xi\right)}{\partial y} = \int_{-a}^{a} \frac{f(\xi)\ y}{(x-\xi)^2 + y^2} d\xi \tag{10}$$

In the limit as $y \to \pm 0$, the function $\frac{y}{(x-\xi)^2+y^2}$ behaves as a delta function: $\pm\pi\,\delta(x-\xi)$. Using the sifting property of delta functions, we find that

$$\int_{-a}^{a} \left[\frac{\partial \Phi}{\partial y}\right]_{y=0^-}^{y=0^+} dx = 2\pi \int_{-a}^{a} f(x)\ dx \tag{11}$$

Substituting Eq. (11) into (9) and rearranging gives the following expression for the charge per unit length on the electrode

$$q = -2\pi\varepsilon_0\varepsilon_r \int_{-a}^{a} f(x)\ dx = -2\pi\varepsilon_0\varepsilon_r Q \tag{12}$$

The charge is directly proportion to the integrated density function, Q, from Eq. (3). From (12), we can find the capacitance per unit length, C, between the plate and the outer pipe (which is grounded).

$$C = \frac{q}{V_0} \tag{13}$$

As the distance between the electrode and casing becomes much smaller than the dimensions of the electrode, the system will tend towards the geometry of a parallel plate capacitor. Its capacitance is expressed as

$$C_P = \frac{\varepsilon_0\varepsilon_r A}{d} \tag{14}$$

where A is the surface area of the electrode plate and ε_r is the relative permittivity of the material between the two plates separated by a distance, d. If the volume between the plates is filled with gas, $\varepsilon_r = 1$, whereas $\varepsilon_r > 1$ if it is filled with a liquid. For a system with a liquid layer and an air layer sandwiched together, the effective capacitance can be expressed by that of two capacitors connected in series, i.e. $C = \frac{C_{\text{gas}} C_{\text{liq}}}{C_{\text{gas}} + C_{\text{liq}}}$. From this, we can expect the capacitance to increase as the electrode approaches the casing and as the thickness of the liquid layer increases, since the overall effective ε_r between the electrode and casing will be increasingly greater than 1. The capacitance should also be higher for higher permittivity liquids, such as water ($\varepsilon_w = 80$), than for low permittivity liquids such as oil ($\varepsilon_{\text{oil}} = 2.2$).

Planar model

Adaptation from real geometry

For simplicity, the system is first modelled in a planar geometry to obtain estimated capacitance measurements using mathematical methods (section 'Theoretical model') and a finite element software, COMSOL multiphysics (section 'COMSOL multiphysics model'). This model can be viewed as an adaptation of the real circular system, where only the top half (and therefore one source) is considered (see Fig. 2).

Theoretical model

General method

The planar system uses Cartesian coordinates (x, y), with the centre of the plate positioned at the origin. For simplicity, the system is assumed to be infinite in x so that there are no vertical boundaries or horizontal domain dimensions to account for. This

allows the Fourier transform of the potential expression to be taken, from which the interaction term U can be obtained. The Fourier transform of U satisfying Laplace's equation, (7), is given by the second-order partial differential equation

$$\frac{\partial^2 \bar{U}(t,y)}{\partial y^2} - t^2\,\bar{U}(t,y) = 0 \tag{15}$$

where

$$\bar{U}(t,y) = \int_{-\infty}^{\infty} e^{it(x-\xi)}\,U(x-\xi,y)\,d(x-\xi) \tag{16}$$

U has different forms depending on whether the interaction potential is taken in the gas region, U_g, or in the liquid region, U_L. The general functions for $\bar{U_L}$ and $\bar{U_g}$ are as follows

$$\bar{U_L} = \kappa_L \cosh((y-h)\,t) + \lambda_L \sinh((y-h)\;\;t) \tag{17}$$

$$\bar{U_g} = \kappa_g \cosh((y-h)\;\;t) + \lambda_g \sinh((y-h)\;\;t) \tag{18}$$

where κ_{L}, λ_{L}, κ_{g}, and λ_{g} are functions depending on t, relative permittivities and the geometry of the system.

Conservation of electric potential, $\phi = \ln r + U$, at the boundaries and the continuity of the normal component of the electric displacement field give four equations:

$$\begin{array}{rl} \ln r + U_L = 0 & ;\quad y = h_2 \\ U_L = U_g & ;\quad y = h \\ \varepsilon_g \dfrac{\partial \varphi_g}{\partial y} = \varepsilon_{\mathrm{L}} \dfrac{\partial \varphi_L}{\partial y} & ;\quad y = h \\ \ln r + U_g = 0 & ;\quad y = -h_1 \end{array} \tag{19}$$

The Fourier transforms of these equations can be solved simultaneously to obtain expressions for the unknown functions. As the plate is surrounded by gas, only U_g is required for the integral equation, and so, only κ_g and λ_g were evaluated. These expressions are given below.

$$\kappa_g = \frac{-\pi\left(\left(\frac{\varepsilon_g}{\varepsilon_L}-1\right)\frac{e^{-h|t|}}{t} - \frac{\varepsilon_g}{\varepsilon_L}\frac{e^{-h_1|t|}}{|t|\sinh((h_1+h)\,t)} - \frac{e^{-h_2|t|}}{|t|\sinh((h_2-h)\,t)}\right)}{\coth((h_2-h)\,t) + \frac{\varepsilon_g}{\varepsilon_L}\coth((h_1+h)\,t)} \tag{20}$$

$$\lambda_g = \frac{\kappa_g \cosh((h_1+h)\,t) - \frac{e^{-h_1|t|}}{|t|}}{\sinh((h_1+h)\,t)} \tag{21}$$

Care was taken to ensure that the integrand of the inverse Fourier transform of $\bar{U_g}$ at $y = 0$ was not singular at $t = 0$, by evaluating the following equation

$$U_g = \frac{1}{2\pi}\int_{-\infty}^{\infty}\left(\bar{U_g} - \bar{U_g^*}\right)e^{i(x-\xi)t}\,dt + U_g^* \tag{22}$$

where $\bar{U_g^*} = \lim_{t\to 0}\,\bar{U_g}$ and is Fourier inverted analytically to obtain U_g^*. $\bar{U_g} - \bar{U_g^*}$ is even in t, and so Eq. (22) can be written

$$U_g = \frac{1}{\pi}\int_0^{\infty}\left(\bar{U}_g - \bar{U}_g^*\right)\cos((x-\xi)t)dt + U_g^* \tag{23}$$

The integrand is evaluated numerically to obtain U_g, which is used to solve the integral Eq. (1). Two different methods were used to solve this equation for electrode charge and are detailed in the next two sub-sections.

Point strength method

The integral equation for this method assumes that the electrode plate is far away from the boundaries, i.e. when the plate is much narrower than its distance to the nearest boundary. Thus, we can say that the interaction with the boundaries is due to an image source induced by a centralised point source of strength Q (defined by Eq. (3)) on the electrode. The dependence of the interaction term U on $(x\text{-}\xi)$ is negligible provided $\frac{2h}{a} \gg 1$, where h is the distance of the plate to the nearest boundary. It can therefore be assumed that U_g on the plate is a constant and is evaluated on the origin $x = 0$, $y = 0$. The plate is assumed to have a width of 2 units, with all geometric parameters scaled accordingly. On $-1 < x < 1$,

$$\int_{-1}^{1} f(\xi)\,\ln|x-\xi|\,d\xi + U_g|_{x=0,y=0} Q = V_0 \tag{24}$$

Substituting in Eq. (2) and $x = \cos(\theta)$ and $\xi = \cos(\psi)$, we find

$$Q = \frac{V_0}{U_g|_{x=0,y=0} - \ln 2} \tag{25}$$

The capacitance of the plate per unit length can be calculated using Eqs. (23), (12) and (13), where $Q = \int_{-1}^{1} f(\xi)\,d\xi$, $F(\xi) = F$ and $a = 1$. Parameters used for the calculation are given in Table 1 (section 'Results and comparison'). Due to the assumptions made, this method will lose accuracy as the plate approaches the liquid layer, but does provide a relatively simple and fast calculation of capacitance.

Integration method

The integral for this more accurate method is the same as Eq. (1), but now, we integrate over the plate along x as well. Making the same substitutions as in the point

Table 1 Parameters used in calculations for the planar model

Parameter	Values used
h_1 (electrode to tool)	44 mm, 47 mm, 51 mm
h_2 (electrode to casing)	11 mm, 8 mm, 4 mm
h (electrode to liquid boundary)	0–2 mm: steps of 0.2 mm
V_0	1 V
ε_g	1
ε_L	2.2 (oil), 89 (water), >100 (salt water)

strength approximation method, $x = \cos(\theta)$ and $\xi = \cos(\psi)$, the integrated equation for the plate, $-1 < x < 1$, is now written

$$F\int_0^{\pi}\int_0^{\pi}\left(\ln|\cos\theta-\cos\psi| + U_g\right)\ d\psi\ \ d\theta = V_0\pi \tag{26}$$

Substituting x and ξ into Eq. (23) and integrating gives

$$\int_0^{\pi}\int_0^{\pi} U_g\ d\psi\ \ d\theta = \int_0^{\pi}\int_0^{\pi} U_g^*\ d\psi\ \ d\theta + \frac{1}{\pi}\int_0^{\pi}\int_0^{\pi}\int_0^{\infty}\cos((\cos\theta-\cos\psi)\,t)\ \left(\bar{U}_g-\bar{U}_g^*\right)\ dt\,d\psi\,d\theta \tag{27}$$

As $\bar{U}_g$ and $\bar{U}_g^*$ have no θ or ψ dependence and as

$$\int_0^{\pi}\cos(t\cos\theta)\ \ d\theta = \pi J_0(t) \tag{28}$$

where $J_0(t)$ is the Bessel function of the first kind, Eq. (27) becomes

$$\int_0^{\pi}\int_0^{\pi} U_g\ d\psi\ \ d\theta = \int_0^{\pi}\int_0^{\pi} U_g^*\ d\psi\ \ d\theta + \int_0^{\infty}\pi\left(J_0(t)\right)^2\ \left(\bar{U}_g-\bar{U}_g^*\right)\ dt \tag{29}$$

F can therefore be calculated via numerical evaluation of Eq. (26) and as $Q = \int_{-1}^{1} f(\xi)\,d\xi = \pi F$, capacitance per unit length can be obtained.

COMSOL multiphysics model

Setup

In COMSOL multiphysics, the geometry in Fig. 2 was built using defined global parameters for h, h_1, h_2, ε_L and V_0, fixing the width of the electrode at 15 mm. Using the Electrostatics module from the AC/DC selection, a block of height $(h_1 + h)$ was defined to be gas, $\varepsilon_g = 1$, and an upper block of height $(h_2 - h)$ was defined as a liquid with a relative permittivity of ε_L. This gave a total height of $h_1 + h_2 = 55$ mm: the distance between the casing and tool. The horizontal length of these domains was finite and chosen to be 0.15 m, such that the total area of this planar system was equal to half the area between the casing and tool in the circular model. A thin rectangular slit of height 0.15 mm and width 15 mm represented the electrode.

The boundary conditions were imposed by setting the potential of the lower block's lower boundary to zero, the edges of the electrode as terminals at voltage V_0 and the top boundary of the upper block as ground, with a potential of zero. Care was taken to build a fine mesh with very many points around the edges of the electrode and with boundary layers within the liquid block so that the parameter h, and hence the liquid layer thickness, could be changed in the study (demonstrated in Fig. 3).

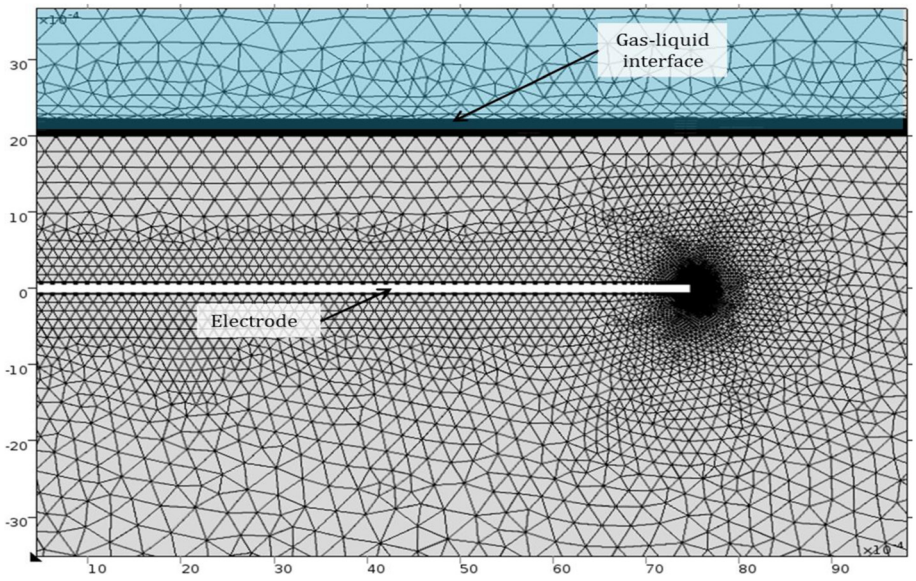

Fig. 3 Snapshot of the mesh built in COMSOL for the planar model studies, showing elements around the electrode end and boundary layers at the gas-liquid interface

Studies

A parametric sweep was created which varied h so that the liquid layer thickness varied from 0 to 2 mm in steps of 0.2 mm. The 'global evaluation' gave a capacitance between the electrode and the casing for each value of h. The programme integrates the electrical energy density over the system to calculate the capacitance [6]. To cross check these values, the line integrals of the perpendicular electric field component across the boundaries of the electrode were taken and summed together to form a closed line integral. From this, the charge on the plate could be calculated using Eq. (26), and so the values for capacitance per unit length using this method were evaluated and compared to the energy density method values. The slight discrepancies between the values are likely due to the singularity of the electric field on the electrode, in which case the energy method COMSOL uses will give more accurate results as it is less dependent on the way the geometry is meshed [6]. These energy method results were calculated for different plate to casing distances and relative permittivities, ε_L, for each liquid.

Results and comparison

The parameters used in the COMSOL model are given in Table 1.

The geometric parameters were scaled down by a factor of 7.5 mm for the theoretical model as the plate is assumed to be of width 2 units.

For the salt water results, the liquid was modelled as a perfect conductor and therefore we set the parameters $h_2 = h$, as though there is no liquid layer and the casing decreases in radius.

General trends in the capacitance results and the difference between calculation methods are demonstrated using the following graphs, Figs. 4 and 5. The methods featured in the graph are the finite element COMSOL model, the theoretical point

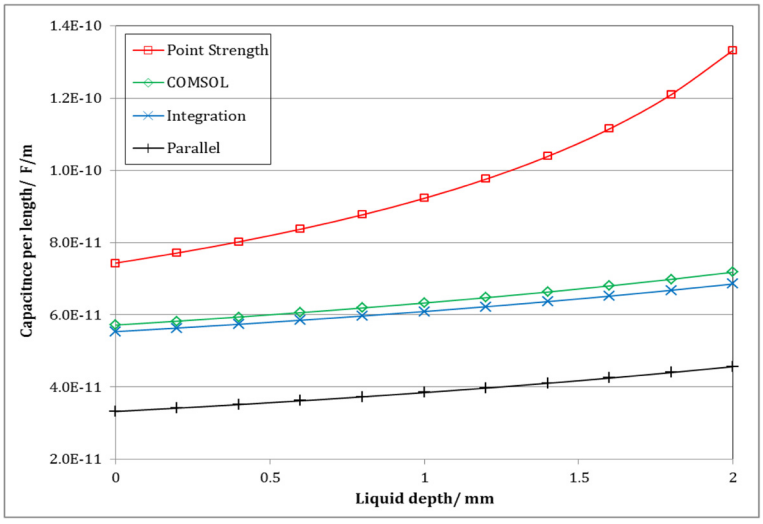

Fig. 4 Planar model: graph of capacitance per metre for varying oil layer thicknesses where the electrode-casing separation is 4 mm, calculated using COMSOL, both theoretical models and a parallel plate approximation

strength and integration theories, and also the parallel plate approximation, as described in the section 'Background theory', Eq. (14), with a gas capacitor and liquid capacitor, which are the same width as the electrode, connected in series. Figure 4 shows the capacitance per unit length for an electrode-casing separation of 4 mm against oil layer thickness, and Fig. 5 shows the variation of capacitance with the electrode-casing distance for both water and oil. Values for salt water are very similar to those for water and so have not been shown on this graph for clarity.

It can be seen in Fig. 4 that capacitance increases superlinearly with the thickness of the liquid present. Figure 5 shows that capacitance is greater, for a given calculation method, when the liquid has a higher permittivity, i.e. the capacitance of a water layer

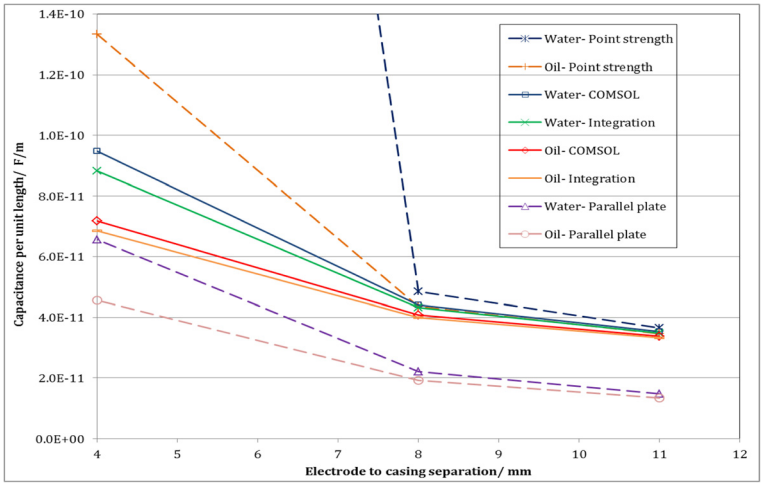

Fig. 5 Planar model: graph of capacitance/metre against electrode-casing distance for a liquid layer of thickness 2 mm, calculated for both water and oil using COMSOL, both theoretical methods and the parallel plate approximation. The value for water-point strength at 4-mm plate-casing separation is 7.7×10^{-10} F/m and so is not displayed on the graph. *Lines* have been drawn between points for clarity only

is greater than that of an oil layer. Decreasing the distance between the electrode and the casing increases the value of capacitance. These relations are all to be expected given that the effective relative permittivity in the area between the electrode and casing increases in each case.

The results from the different methods are similar in the trends discussed earlier; however, the magnitudes of the capacitances calculated are very different.

At $h_2 = 4$ mm, the approximation for the point strength theoretical model (that the distance of the electrode to the liquid-gas boundary, $h \gg 3.75$ mm) clearly breaks down (Fig. 4). It can be seen in Fig. 5 that this method tends towards the COMSOL and theoretical integration methods as h_2 increases, agreeing with the method's approximation condition.

The results of the two most accurate methods of the study, the mathematical integration method and the COMSOL model, agree quite closely with a difference of only 1 to 7 %. This error increases as the electrode-casing separation decreases and also varies with the permittivity and thickness of the liquid layer. This is not too surprising as these variables increase the sensitivity of the finite element method in COMSOL, requiring more elements as regions become narrower for example. Error may also be due to the singular electric fields at the corners of the plate and potential discontinuities at the boundaries, which are more difficult to model using finite elements (see [6]) but are dealt with exactly in the theoretical models.

The integration method capacitance values are consistently lower than the COMSOL values. This is due to the electrode in the COMSOL model having a finite thickness, rather than being infinitesimally thin, unlike in the theoretical methods. The voltage on the vertical sides of the electrode was also set to V_0, and as this would give the electrode a larger effective length, the capacitance is higher.

From Fig. 4, we can see that the capacitance values for the parallel plate approximation are significantly lower than the COMSOL and integration theory results, but show a very similar trend. Values are much lower as it does not account for the interaction of the electrode with the casing and liquid which extend beyond the ends of the electrode or the interaction with the grounded tool.

The parallel plate capacitance equation, (14), only holds for when the lengths of the plates are much larger than plate separation, as edge effects are not taken into account in the derivation of this formula. This is likely to be why discrepancies are around 60 % lower for the 11-mm separation, but around 30 % lower for the 4-mm gap, where the plate width is several times larger than this distance.

For practical implementation, the capacitance sensor can be calibrated by measuring capacitance without the presence of a liquid layer, C_0, for a given electrode position, and so detection of liquid would be due to measuring a percentage change in the capacitance. Hence, it is useful to gauge the sensitivity of the measurement by calculating $\frac{\Delta C}{C_0}$ where ΔC is the change in capacitance, $C - C_0$. Figure 6 represents the sensitivity of the capacitance measurement with thickness of the liquid layer for an 11-mm electrode-casing separation. The percentage increase and sensitivity to liquid layer thickness is far higher for the measurements

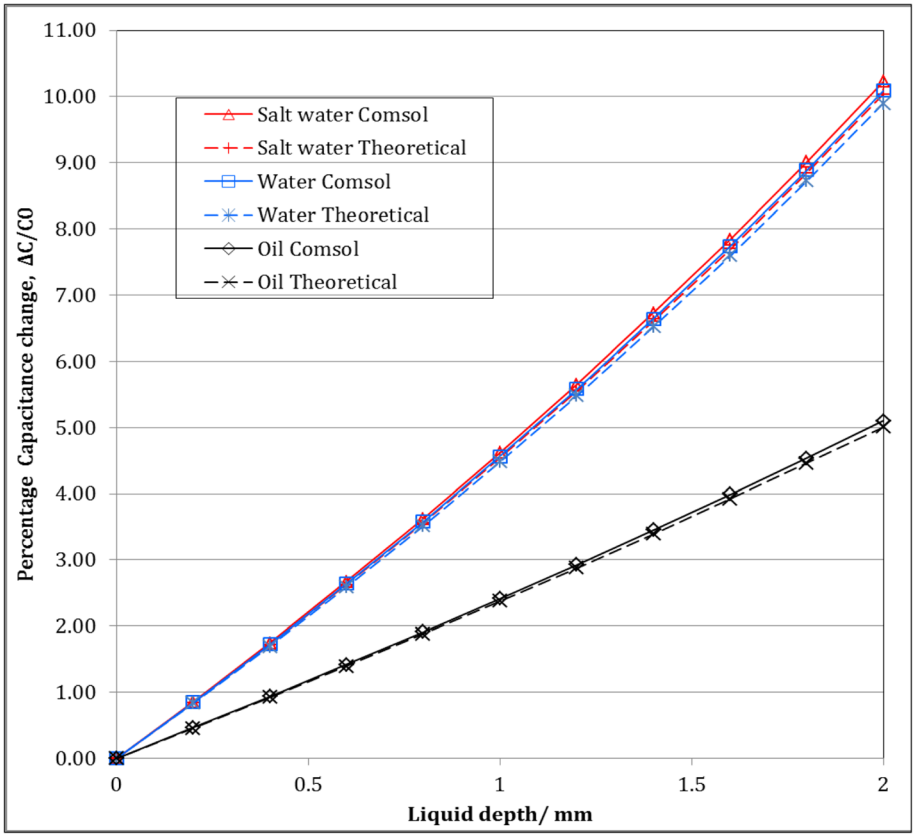

Fig. 6 Planar model: percentage capacitance change against liquid layer thickness for 11-mm plate-casing separation

using a smaller electrode-casing separation, reaching around 25 % for oil and around 65 % for water at 4-mm separation compared to an 11-mm separation which only reaches 5 % for oil and 10 % for water, as shown in Fig. 6.

It can be seen from Fig. 6 that one measurement of capacitance will not necessarily be enough to determine the thickness of the liquid layer if the liquid is unknown, as below a certain capacitance value, there will be a corresponding thickness for both liquids. In other words, a horizontal line drawn across the graph will cross both the oil and water lines. However, if the measurement is above a certain value, i.e. the capacitance when a 2-mm oil layer is present, water or salt water can be identified unambiguously and thickness can be calculated, assuming 2 mm is the maximum liquid depth. The minimum capacitance changes needed to identify water are given in Table 2.

These measurements assume that 2 mm is the maximum liquid depth. Any larger thicknesses can be modelled, and a new minimum capacitance can be found.

Table 2 Minimum percentage capacitance change needed to identify water presence according to the planar model

Electrode to casing distance/ mm	Minimum percentage change in capacitance (%)
11	6
8	9
4	26

If the type of liquid is known, the thickness of liquid on the inside of the casing wall can be estimated. Further discussion on the practical implications of the capacitance results can be found in the section 'Results and comparison' in the results for the more realistic circular model.

Circular model

Geometry

The cross section of the real geometry was used for this model, shown in Fig. 7 below.

Theoretical model

General method

A Fourier transform cannot be used for this model as there are no infinite limits in the geometry. We instead use the Fourier series expansion of the potential using polar coordinates, (r, θ), in order to find the interaction potential terms and the integral of the source density, $f(r_0, \theta_0)$, over the electrode, where (r_0, θ_0) is the position of the point source. r is the distance from the origin, which is the centre of the tool, and θ is clockwise from the origin with $\theta = 0$ at the centre of the top electrode.

The potential due to a point source in an infinite medium, ϕ^*, is written in polar coordinates as

$$\varphi^* = \frac{1}{2}\ln\left(r^2 + {r_0}^2 - 2rr_0\cos(\theta - \theta_0)\right) \tag{30}$$

Equation (30) can be written as two Fourier series, the first is when $r < r_0$ and the second is when $r > r_0$.

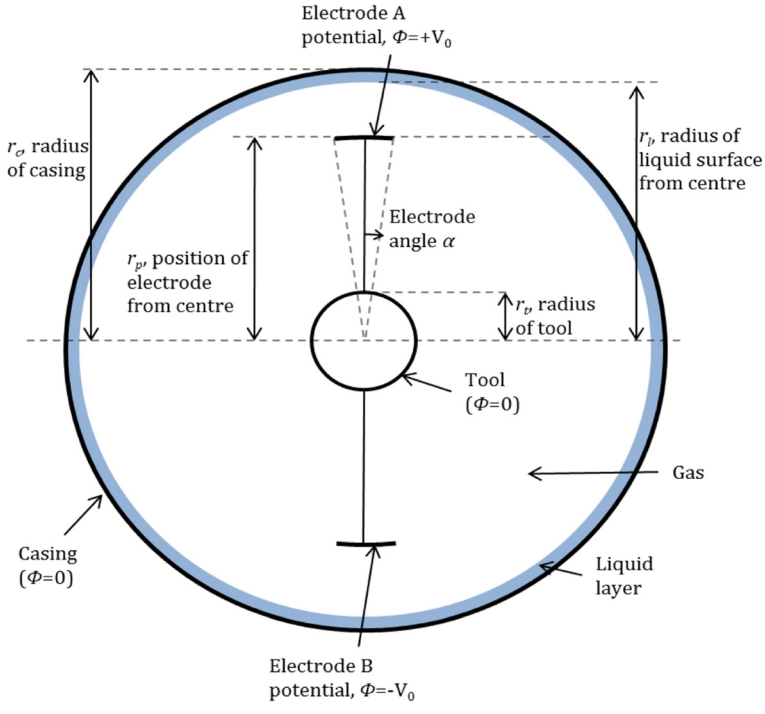

Fig. 7 Geometry and boundary conditions of the circular model

$$\varphi_s^* = \ln r_0 + \sum_{m=1}^{\infty} \frac{-1}{m} \left(\frac{r}{r_0}\right)^m \cos(m\ (\theta - \theta_0)) \ ; \quad r < r_0 \tag{31}$$

$$\varphi_l^* = \ln r + \sum_{m=1}^{\infty} \frac{-1}{m} \left(\frac{r_0}{r}\right)^m \cos(m\ (\theta - \theta_0)) \ ; \quad r > r_0 \tag{32}$$

U has different forms depending on whether the interaction potential is taken in the gas region, U_g, or in the liquid region, U_L. The general Fourier series solutions of Laplace's equation for U_g and U_L are given below as Eqs. (33) and (34)

$$U_g = \kappa_{g0} \ln r + \lambda_{g0} + \sum_{m=1}^{\infty} \left(\lambda_{gm} r^m + \mu_{gm} r^{-m}\right) \cos(m\ (\theta - \theta_0)) \tag{33}$$

$$U_L = \kappa_{L0} \ln r + \lambda_{L0} + \sum_{m=1}^{\infty} (\lambda_{Lm} r^m + \mu_{Lm} r^{-m}) \cos(m\ (\theta - \theta_0)) \tag{34}$$

where κ_{L0}, κ_{g0}, λ_{g0}, λ_{L0}, λ_{gm}, λ_{Lm}, μ_{gm} and μ_{Lm} are functions depending on m and the geometry of the system.

These functions were found using the boundary conditions, shown below in equation set (35), comparing the coefficients and solving simultaneous equations.

$$\begin{aligned} \varphi_s^* + U_g &= 0 \quad ; \ r = r_t \\ U_L &= U_g \quad ; \ r = r_l \\ \varepsilon_g \left(\frac{\partial \varphi_l^*}{\partial r} + \frac{\partial U_g}{\partial r}\right) &= \varepsilon_L \left(\frac{\partial \varphi_l^*}{\partial r} + \frac{\partial U_L}{\partial r}\right) \ ; \ r = r_l \\ \varphi_l^* + U_L &= 0 \quad ; \ r = r_c \end{aligned} \tag{35}$$

As with the planar model, only U_g is required for the integral equation and so only κ_{g0}, λ_{g0}, λ_{gm} and μ_{gm} were calculated. These expressions are given below

$$\kappa_{g0} = \frac{\left(1 - \frac{\varepsilon_g}{\varepsilon_L}\right) \ln r_l + \frac{\varepsilon_g}{\varepsilon_L} \ln r_c - \ln r_0}{\ln r_t - \left(1 - \frac{\varepsilon_g}{\varepsilon_L}\right) \ln r_l - \frac{\varepsilon_g}{\varepsilon_L} \ln r_c} \tag{36}$$

$$\lambda_{g0} = \frac{\left(\left(1 - \frac{\varepsilon_g}{\varepsilon_L}\right) \ln r_l + \frac{\varepsilon_g}{\varepsilon_L} \ln r_c\right)(\ln r_0 - \ln r_t)}{\ln r_t - \left(1 - \frac{\varepsilon_g}{\varepsilon_L}\right) \ln r_l - \frac{\varepsilon_g}{\varepsilon_L} \ln r_c} \tag{37}$$

$$\lambda_{gm} = \frac{-\left(\frac{\varepsilon_g}{\varepsilon_L}\left(\left(\frac{r_l}{r_c}\right)^{2m} - 1\right) + \left(\frac{r_l}{r_c}\right)^{2m} + 1\right)\left(\left(\frac{r_0}{r_c}\right)^{2m} - \left(\frac{r_t}{r_c}\right)^{2m}\right)}{m r_0{}^m \left(\frac{\varepsilon_g}{\varepsilon_L}\left(\left(\frac{r_l}{r_c}\right)^{2m} + \left(\frac{r_l}{r_c}\right)^{2m}\right)\left(\left(\frac{r_l}{r_c}\right)^{2m} - 1\right) + \left(\left(\frac{r_l}{r_c}\right)^{2m} + 1\right)\left(\left(\frac{r_l}{r_c}\right)^{2m} - \left(\frac{r_l}{r_c}\right)^{2m}\right)\right)} \tag{38}$$

$$\mu_{gm} = \frac{r_t{}^{2m}}{m r_0{}^m} \frac{1 + \left(\frac{\varepsilon_g}{\varepsilon_L}\left(\left(\frac{r_l}{r_c}\right)^{2m} - 1\right) + \left(\frac{r_l}{r_c}\right)^{2m} + 1\right)\left(\left(\frac{r_0}{r_c}\right)^{2m} - \left(\frac{r_t}{r_c}\right)^{2m}\right)}{\left(\frac{\varepsilon_g}{\varepsilon_L}\left(\left(\frac{r_l}{r_c}\right)^{2m} + \left(\frac{r_l}{r_c}\right)^{2m}\right)\left(\left(\frac{r_l}{r_c}\right)^{2m} - 1\right) + \left(\left(\frac{r_l}{r_c}\right)^{2m} + 1\right)\left(\left(\frac{r_l}{r_c}\right)^{2m} - \left(\frac{r_l}{r_c}\right)^{2m}\right)\right)} \tag{39}$$

Integration method

Only the integration method was used for the circular theoretical model, as the results obtained for the point strength method are inaccurate for the dimensions of this study

(see the section 'Results and comparison') when the distance of the electrode to the liquid layer, h, is $h \not\gg \frac{a}{2}$, where a is the width of the electrode. Expressions for the point strength method can be obtained easily using the same method as in the section 'Point strength method', approximating the electrodes to be flat.

The curvature of the electrode for this model is approximated to having a radius of r_p but with a fixed arc length of 15 mm. The top electrode A is at a radius of $r_\mathrm{p} = r_\mathrm{A}$ and spans $-\alpha < \theta < \alpha$, and the lower electrode B is at a radius of $r_\mathrm{p} = r_\mathrm{B}$ and spans $\beta_1 < \theta < \beta_2$. We assume that the charge density distributions (Eq. (2)) take the forms $f_A(\theta_{0A}) = \frac{F_A}{\left(\alpha^2-\theta_{0A}{}^2\right)^{\frac{1}{2}}}$ and $f_B(\theta_{0B}) = \frac{F_B}{((\beta_2-\theta_{0B})(\theta_{0B}-\beta_1))^{\frac{1}{2}}}$ where F_A and F_B are constant along the electrodes.

For the two sources, the integral equation is similar to that in Eq. (1) but now includes both sources. Potential on electrode A, $-\alpha < \theta < \alpha$, is

$$\int_{-\alpha}^{\alpha} f_A(\theta_{0A})\left(\varphi_A^*|_{r_A} + U_A|_{r_A}\right)d\theta_{0A} + \int_{\beta_1}^{\beta_2} f_B(\theta_{0B})\left(\varphi_B^*|_{r_A} + U_B|_{r_A}\right)d\theta_{0B} = +V_0 \tag{40}$$

We then substitute $\theta = \alpha\cos(\psi)$, $\theta_{0\mathrm{A}} = \alpha\cos(\psi_A)$, $\theta_{0\mathrm{B}} = \left(\frac{\beta_1+\beta_2}{2}\right) + \left(\frac{\beta_2-\beta_1}{2}\right)\cos(\psi_\mathrm{B})$ and integrate $0 < \psi < \pi$, which is equivalent to integrating $-\alpha < \theta < \alpha$. This gives

$$\begin{aligned} &F_A\int_0^{\pi}\int_0^{\pi} \varphi_A^*|_{r_A}\, d\psi_A\, d\psi + F_A\int_0^{\pi}\int_0^{\pi} U_A|_{r_A}\, d\psi_A\, d\psi + F_B\int_0^{\pi}\int_0^{\pi} \varphi_B^*|_{r_A}\, d\psi_B\, d\psi \\ &\quad + F_B\int_0^{\pi}\int_0^{\pi} U_B|_{r_A}\, d\psi_B\, d\psi \\ &\quad = +V_0\pi \end{aligned} \tag{41}$$

On plate B, the integral equation is similar to Eq. (41) but evaluated on r_B and the right hand side is $-\pi V_0$, with the substitution $\theta = \left(\frac{\beta_1+\beta_2}{2}\right) + \left(\frac{\beta_2-\beta_1}{2}\right)\cos(\psi)$ instead. These two integral equations can be used to solve for F_A and F_B. The double integrals over the ϕ^* terms are evaluated numerically, and the double integrals over U can be expressed analytically using the Bessel function identity (section 'Theoretical model', Eq. (28)).

$$\int_0^{\pi}\int_0^{\pi} U_x|_y \; d\psi_x d\psi = \pi^2\left[\begin{array}{c} {}_{Kg0}|_{r_x}\ln r_y + \lambda_{g0}|_{r_x} \\ +\sum_{m=1}^{\infty}\left(\lambda_{gm}|_{r_x} r_y{}^m + \mu_{gm}|_{r_x} r_y{}^{-m}\right) J_0(m\delta)\;\; J_0(m\gamma)\;\; \cos(m(\omega-\chi)) \end{array}\right] \tag{42}$$

Here, x and y represent plate A or B and $\theta = (\delta\cos\psi + \omega)$ and $\theta_{0x} = (\gamma\cos\psi_x + \chi)$. F_A and F_B are given by

$$F_B = \frac{-\pi V_0\left(I\left[\varphi_A^*|_{r_B} + U_A|_{r_B}\right] + I\left[\varphi_A^*|_{r_A} + U_A|_{r_A}\right]\right)}{I\left[\varphi_B^*|_{r_B} + U_B|_{r_B}\right]\;\; I\left[\varphi_A^*|_{r_A} + U_A|_{r_A}\right] - I\left[\varphi_A^*|_{r_B} + U_A|_{r_B}\right]\;\; I\left[\varphi_B^*|_{r_A} + U_B|_{r_A}\right]} \tag{43}$$

$$F_A = \frac{\pi V_0 - F_B \; I\left[\varphi_B^*|_{r_A} + U_B|_{r_A}\right]}{I\left[\varphi_A^*|_{r_A} + U_A|_{r_A}\right]} \tag{44}$$

In these equations, I [...] is the double integral from 0 to π of ψ and ψ_x, where x is the source electrode.

Thus, the capacitance per unit length between each plate and the casing can be computed.

COMSOL model

Setup

Using COMSOL multiphysics, the geometry in Fig. 7 was built using defined global parameters for r_t, r_p, r_l, r_c, ε_L and V_0, fixing the width of the electrode at 15 mm and the curvature to radius r_c. Unlike the theoretical model, where analytical solutions would have been very difficult to obtain without using the electrode's radial position as the curvature of the electrode, we can use a more realistic setup here with a fixed curvature, as it is unlikely to vary with position. Using the Electrostatics module from the AC/DC selection, the annulus between radius r_t and r_l was defined to be gas, $\varepsilon_g = 1$, and the outer annulus between radius r_l and r_c was defined as a liquid with a relative permittivity of ε_L. Two thin curved slits at radius r_p and curvature r_c, arc length 15 mm and positioned 180° to each other, represented the electrodes. The boundary conditions were imposed as before by setting the potential of the tool surface to zero, the edges of the electrodes as terminals at voltage V_0 on the top electrode and $-V_0$ on the bottom and the casing as ground, with a potential of zero. The mesh was built finely with many points around the edges of the electrode and with boundary layers within the liquid annulus so that the liquid thickness could be changed in the study.

Studies

A parametric sweep was created which varied r_l so that the liquid thickness varied from 0 to 2 mm in steps of 0.2 mm. The 'global evaluation' was used to give the capacitance between an electrode and the casing for each value of r_l, which is the same as the method used for the planar model.

Results and comparison

The parameters used in the COMSOL model are given in Table 3.

Table 3 Parameters used in circular model calculations

Parameter	Values used
r_t (tool radius)	21 mm
r_p (electrode radial position)	65 mm, 68 mm, 72 mm
r_l (gas-liquid boundary radius)	74–76 mm in steps of 0.2 mm
r_c (casing radius)	76 mm
V_0	1 V
ε_g	1
ε_L	2.2 (oil), 89 (water), >100 (salt water)
L (length of electrode along z-axis)	20 cm

The geometric parameters do not need to be scaled for the theoretical results as the widths of the plates have already been taken into account. For α in the theoretical models, the expression $\alpha = \frac{15}{2r_A}$, where $r_p = r_A = r_B$ is in millimetres, is used as the curvature varies and the arc length is constant. The angular position of the bottom electrode was set to $\beta_1 = \pi - \alpha$ and $\beta_2 = \pi + \alpha$. For the salt water results, the liquid was modelled as a perfect conductor and therefore we set the parameters $r_c = r_l$, as though there is no liquid layer and the casing decreases in radius. Data was not produced for the point strength approximation method as we know that the integration method gives far more accurate answers from the planar model results (section 'Results and comparison').

The absolute value of capacitance was calculated for an electrode with a length L, perpendicular to the 2D cross section, of 20 cm, for distances between the electrode and casing of 11, 8, and 4 mm, respectively.

The general trends in capacitance are shown in Figs. 8 and 9 and are the same as those of the planar model. The capacitance increases with permittivity and thickness of the liquid and with decreasing electrode-casing separation. Agreement between the theoretical integration method and the COMSOL model results is still quite good, with similar discrepancies of 1 to 8 %, increasing with capacitance. Possible causes of these discrepancies are discussed in the section 'Results and comparison'.

Capacitance sensitivities, $\frac{\Delta C}{C_0}$, reach around 25 % for oil and around 65 % for water for a 4-mm electrode-casing separation, which is much greater than for 11 mm, which

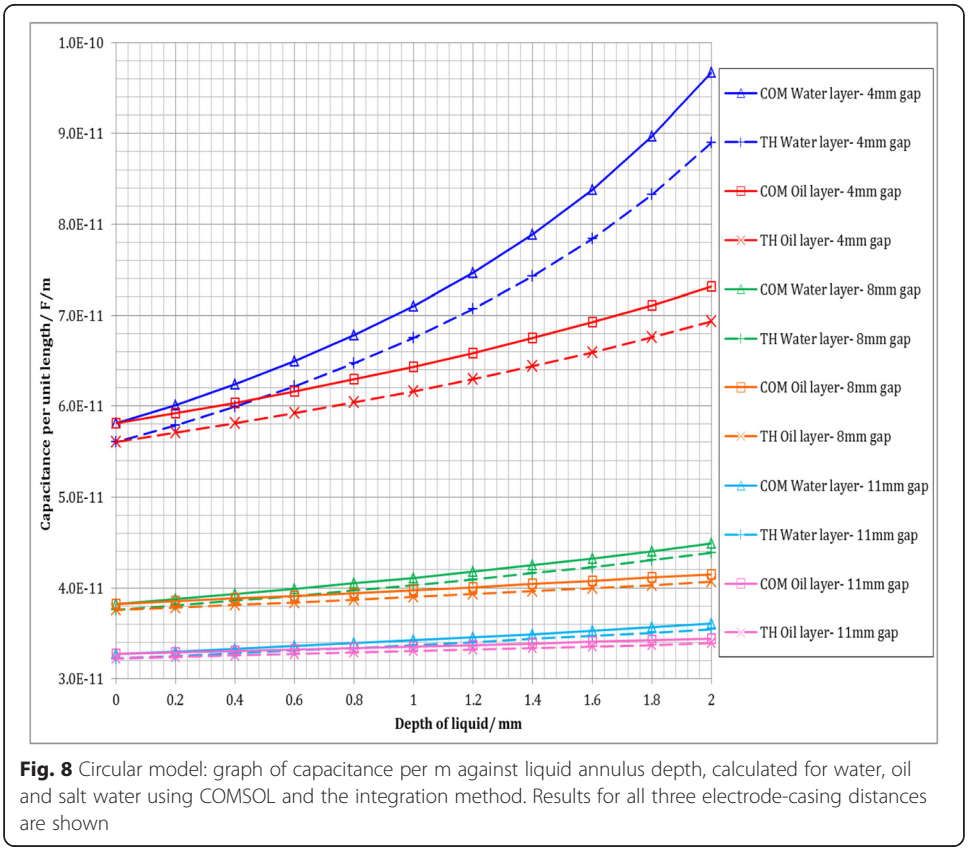

Fig. 8 Circular model: graph of capacitance per m against liquid annulus depth, calculated for water, oil and salt water using COMSOL and the integration method. Results for all three electrode-casing distances are shown

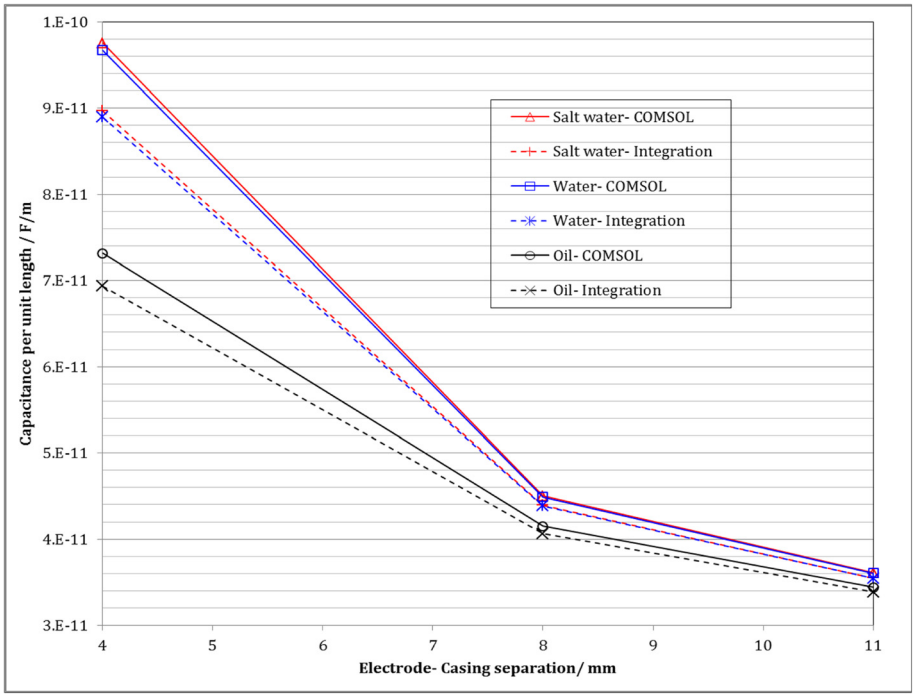

Fig. 9 Circular model: graph of capacitance per m against electrode-casing separation for a liquid layer of thickness 2 mm, calculated for salt water, water and oil using COMSOL and the integration method. *Lines* have been drawn between points for clarity only

only reaches 5 % for oil and 10 % for water. These values are similar to the percentage increases found for the planar model. The minimum percentage changes in capacitance needed to distinguish between oil and water are given in Table 4. These values assume a maximum liquid layer thickness of 2 mm and are the same as those in Table 2, rounding to the highest integer.

The accuracy to which we can measure liquid annulus thickness depends on the resolution of the capacitance sensor. Assuming a minimum detectable capacitance change of $\delta C = 0.1$ pF (see the 'Introduction' section), the resolution of liquid depth that can be calculated. As the relation of capacitance to liquid depth is superlinear, the minimum resolution, in other words the largest uncertainty in depth change we could obtain, is the depth corresponding to the first detected change in capacitance. This depth resolution, $\delta d_{\min}$, can be expressed as $d_{\min} = d(C = C_0 + \delta C)$ and is demonstrated in Fig. 10. The thickness $\delta d_{\min}$ is the minimum thickness of liquid needed to for a change in capacitance to be registered by the sensor.

Figure 10 shows that, given a capacitance measurement, an error in the liquid depth deduced can be found. Table 5 below gives the minimum depth resolution of the liquid

Table 4 Minimum percentage capacitance change needed to identify water presence according to the circular model

Electrode to casing distance/mm	Minimum percentage change in capacitance (%)
11	6
8	9
4	25

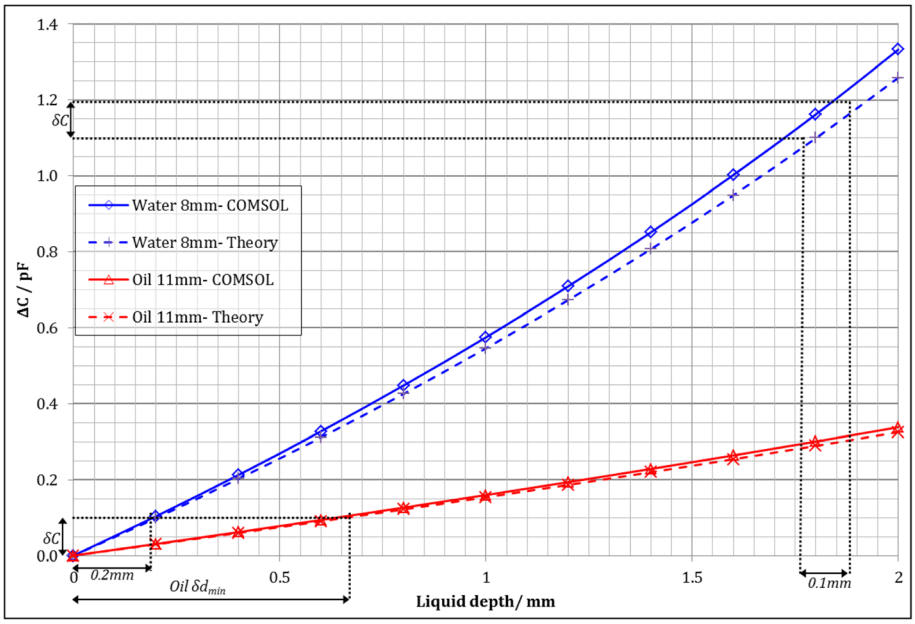

Fig. 10 Circular model: demonstration of finding depth resolution using a graph of ΔC against liquid depth for two example results. It can be seen from the water graph that the depth resolution decreases as the liquid layer increases (here from 0.2 to 0.1 mm). $\delta d_{\min}$ is shown for the oil graph and $\delta C = 0.1$ pF

annulus, using an electrode of size 15 mm × 200 mm. COMSOL and theoretical values were averaged to find $\delta d_{\min}$ at $\Delta C = \delta C = 0.1$ pF.

Using an 11-mm separation between the electrode and casing will not only give small capacitance percentage changes but will also require relatively thick liquid annuli to be registered by the sensor. The smallest detectable depth for oil with an 11-mm separation is around 30 % of the assumed maximum liquid thickness of 2 mm, whereas using an electrode-casing separation of 4 mm allows detection of a water layer of thickness 0.05 mm, 3 % of the maximum thickness. Resolution is better for smaller electrode-casing distances and the sensor will be more sensitive to higher permittivity liquids.

When considering the practical implications of the results, the usefulness of the models must be evaluated. The similarity of the measurement conditions to those modelled may have a great effect on the accuracy of the predicted capacitance and liquid depth estimates. For example, the relative permittivity of a flowing hot gas may vary by as much as 10 %, and the assumptions that the liquid annulus only consists of one material and has a continuous thickness around the wellbore are not entirely realistic. Modelling the system in 2D implicitly assumes that this cross section is constant along the z-axis. In reality, the edges of the electrode along z and the variation of liquid thickness down the wellbore will affect the measured

Table 5 Minimum oil and water thickness resolutions for different electrode-casing separations

Electrode to casing distance/mm	Minimum oil resolution $\delta d_{\min}$/mm	Minimum water resolution $\delta d_{\min}$/mm
11	0.65	0.36
8	0.36	0.20
4	0.10	0.05

capacitance. These results should be compared to laboratory experiments using the production logging tool to check the accuracy. The methods used in this study, especially the mathematical integration method, provide useful estimates of measureable capacitance and have the potential to be used in downhole measurements so long as sufficient calibration is performed.

Overall conclusions

The proposed capacitance measurement system has been modelled for two different geometries, and two different mathematical models have been developed, one approximating the interaction potential as being due to a source far from the boundaries and the other a more accurate method where the interaction potential term is integrated over the electrode. The circular model is a more accurate representation of the real system, and so the results will be more realistic than those from the planar model. Despite this, there is generally quite good agreement between the two different geometries. The theoretical method which gives an approximate solution by satisfying on average the potential integral equation is far more accurate than the point strength method, especially when the electrode tends towards the liquid layer where the far-field approximation used breaks down.

Reasonably good agreement is obtained between the COMSOL finite element model and the integration method, showing that this mathematical model gives realistic results. Percentage discrepancies between the two methods increase with capacitance, from 1.5 % for 0.2 mm oil layer with an 11-mm electrode-casing separation to 8 % for a 2-mm salt water layer with a 4-mm separation. This issue can be reduced by calibrating against a dry condition capacitance measurement and measuring the percentage capacitance change instead.

Generally, the capacitance and measurement sensitivity were found to increase with the depth and permittivity of the liquid and with proximity of the electrode to the casing, as expected. For the example geometry used in this paper, capacitance per unit length values ranged from 32 pF/m with a sensitivity of 0.8 % (for 0.2 mm of oil using 11-mm electrode-casing gap) up to 93 pF/m with a sensitivity of 60 % (for 2-mm layer of water, measured with the electrode 11 mm from the casing).

On a practical level, one of the main issues of the measurement system is the large overlap between values of the capacitance of oil and water for different thicknesses. A capacitance value is likely to give two different thicknesses depending on which liquid is present, and so another independent measurement of either the thickness or the relative permittivity of the liquid should be added to fully characterise the liquid layer.

If the liquid is known, the liquid depth can be estimated from a capacitance measurement. The accuracy of this depth depends on the resolution of the capacitance sensor. Assuming that an electrode of size 15 mm × 200mm is used and that the minimum capacitance change a downhole electronics circuit can detect is 0.1 pF, the minimum liquid depth that can be registered by the sensor range from 0.05 mm of water (using a 4-mm electrode-casing separation) to 0.65 mm of oil (using an 11-mm electrode-casing

separation). These values also represent the largest errors in deduced depth, as the depth resolution improves with increasing capacitance.

Overall, the theoretical method developed is useful and could provide fast real-time analysis for a downhole capacitance sensor. The results should be checked against experimental measurements, but, with careful calibration, the model could potentially be used to detect liquids with a relatively small range of error, provided the electrode is close enough to the liquid annulus.

Competing interests
The authors declare that they have no competing interests.

Authors' contributions
Both authors were responsible for the general theory. CA for the analytical methods and RH for the comsol applications. Both authors read and approved the final manuscript.

Acknowledgements
We would like to thank Dr S. Huang and Dr A. Meredith for helpful discussions and Schlumberger Gould Research for their permission to publish this paper.

Author details
[1]Schlumberger Gould Research Center, Cambridge, UK. [2]Department of Mathematics, Imperial College London, 180 Queen's Gate, London SW7 2AZ, UK. [3]Sidney Sussex College, Cambridge University, Cambridge, UK.

Received: 5 November 2015 Accepted: 5 April 2016
Published online: 26 May 2016

References

1. Mustafa HD, Abdouche G, Khedr OH, Elkadi A, Al-Mutairi AM (2005) A new production logging tool allows a superior mapping of the fluid velocities and holdups inside the well bore. SPE-93556-MS, SPE Middle East Oil and Gas Show and Conference, 12-15 March, Bahrain
2. Kjaersgaard-Rasmussen J (2010) Inside-out electrical capacitance tomography for downhole multiphase flow evaluation, PhD Thesis, DTU Mechnical Engineering
3. COMSOL (2011) Multiphysics ® (Version 4.3) [Software]. COMSOL Inc, Burlington
4. Mikhlin SG (1964) Integral equations and their applications to certain problems in mechanics, mathematical physics, and technology., Macmillan
5. Atkinson C (1972) On dislocation densities and stress singularities associated with cracks and pile-ups in inhomogeneous media. Int J Eng Sci 10:45–71
6. COMSOL, Electromagnetics Module's User Guide Version 3.2, 2005